

Chapter 3

Methodology

3.1 Electron crystallography

The electron wave function $\Psi(\vec{r}, t)$ satisfies the Schrödinger wave equation,

$$-\frac{\hbar^2}{2m}\nabla^2\Psi + V(\vec{r})\Psi = i\hbar\frac{\partial\Psi}{\partial t} \quad . \quad (3.1)$$

In free space the potential $V(\vec{r}) = 0$, the electron energy eigenfunction has the form of a plane wave propagating in the direction of wave vector \vec{k} as

$$\Psi = \Psi_0 \exp(2\pi i(\vec{k} \cdot \vec{r} - \omega t)) \quad , \quad (3.2)$$

where $h\omega = E$ is the electron kinetic energy and $k = 1/\lambda$ is the electron wave number.

In high-energy electron diffraction studies, the electrons used have velocity between $0.1c$ and $0.99c$, where c is the speed of light and the relativistic effects are not negligible. Equation (3.1) can be corrected for relativistic effects by replacing the electron rest mass by its relativistic mass, and the energy E by $E \left(\frac{m_0}{m}\right) \left(1 + \frac{E}{2m_0c^2}\right) = \frac{h^2k_0^2}{2m}$, where \vec{k}_0 is the relativistic wave vector. The wavelength λ is thus given by

$$\lambda = \left[\frac{2m_0E}{h^2} \left(1 + \frac{E}{2m_0c^2} \right) \right]^{-1/2} = \frac{12.2643}{\sqrt{E + 0.97845 \times 10^{-6} E^2}} \quad . \quad (3.3)$$

In our UEC experiment, the electrons generated from the electron gun have energy $E = 30$ keV, and their wavelength is $\lambda = 0.0698$ Å from equation (3.3).

For an incident plane wave of the form (3.2), in the kinematic approximation, the wave function at a distance far from the sample ($r \gg r'$) is [3, 33, 34]

$$\Psi(\vec{r}) \approx \Psi_0(\vec{r}) + \frac{\exp(2\pi i k_0 r)}{r} f^{(B)}(\vec{k}, \vec{k}_0) \quad ,$$

where $f^{(B)}(\vec{k}, \vec{k}_0) = f^{(B)}(\vec{k} - \vec{k}_0)$ is the Born or the kinematic scattering amplitude given by the Fourier transform of the potential $V(\vec{r})$,

$$f^{(B)}(\vec{q}) = -\frac{m}{2\pi\hbar^2} \int V(\vec{r}') \exp[-2\pi i \vec{q} \cdot \vec{r}'] d\vec{r}' \quad ,$$

here $\vec{q} \equiv \vec{k} - \vec{k}_0$. The space spanned by all \vec{q} is the reciprocal space, in respect to the real or direct space of \vec{r} .

In principle, if the Born scattering amplitude could be obtained from the diffraction experiment, an inverse Fourier transform would give the real space potential distribution. Since the potential is generated by the electrons and nuclei, the position of the atoms in real space could then be solved. However, in real experiments, only the intensity of the electron beam is obtained, i.e., only $|\Psi^*(\vec{r})\Psi(\vec{r})|$ is known, and the phase of the diffracted beams cannot be directly obtained. There are considerable efforts to solve for the phase by indirect experimental and mathematical methods.

For a single atom, the atomic scattering factor $f^{(e)}(s)$ is the Fourier transform of the atomic potential $\varphi(\vec{r})$,

$$f^{(e)}(s) = \frac{2\pi m e}{h^2} \int \varphi(\vec{r}) \exp(2\pi i \vec{q} \cdot \vec{r}) d\vec{r} \quad ,$$

where $s = 2\pi |\vec{q}|$ is conventional for gas diffraction. The atomic scattering factor is tabulated in the International Tables for Crystallography. Alternatively, it can be calculated using an analytical fit of the form

$$f^{(e)}(s) = \sum_{j=1}^n a_j \exp(-b_j s^2) \quad ,$$

where a_j and b_j are fitting parameters, and $n=3, 4$ and 5 has been used in literature

[34].

For a collection of atoms such as molecules or a unit cell in the crystal, if the effect of redistribution of valence electrons due to chemical bonding is neglected, the kinematic amplitude of scattering is given by the Fourier transform of the sum of the potential field from single atoms,

$$F(\vec{q}) = \sum_j f_j^{(e)}(s) \exp(-2\pi i \vec{q} \cdot \vec{r}_j) \quad . \quad (3.4)$$

And the diffracted electron intensity is given by

$$I(\vec{q}) = F^*(\vec{q})F(\vec{q}) = \sum_i \sum_j f_i^*(s) f_j(s) \exp[2\pi i \vec{q} \cdot (\vec{r}_i - \vec{r}_j)] \quad . \quad (3.5)$$

Gases, liquids and amorphous solids are statistically isotropic. They are described by interatomic distances $\vec{r}_{ij} = \vec{r}_i - \vec{r}_j$, which can be assumed to take all orientations in space with equal probability. The diffracted intensity given by the time-averaged, spherically symmetrical distribution is

$$I(q) = \sum_i \sum_j f_i^*(s) f_j(s) \frac{\sin sr_{ij}}{sr_{ij}} \quad .$$

This is the Debye scattering equation. The sum of the terms with $i = j$ is the so-called atomic scattering background, which is a smoothly falling intensity from all atoms considered separately, $\sum_i |f_i(s)|^2$. The sum of the terms with $i \neq j$ give oscillations of the molecular scattering denoted by $I_m(s)$, experimentally obtained by subtraction of the smooth background. The Fourier transform of this function gives the radial distribution function

$$D(r) = \int_0^\infty s I_m(s) \sin(sr) ds \quad ,$$

which directly shows the distribution of probabilities for the occurrence of the interatomic distance r , weighted by the scattering strengths of the contributing atoms. From this, the interatomic distances and hence the structure may be derived.

In a crystal, a unit cell is repeated in a periodic array in three dimensions. The unit cell may contain single atom, group of atoms or molecules. Let $\phi(\vec{r})$ denotes the potential in the unit cell, the potential of the entire crystal is then given by

$$V(\vec{r}) = \sum_{n_1} \sum_{n_2} \sum_{n_3} \phi(\vec{r} - n_1\vec{a} - n_2\vec{b} - n_3\vec{c}) \quad ,$$

where \vec{a} , \vec{b} and \vec{c} are the lattice vectors. The kinematic scattering amplitude is the Fourier transform of this potential, namely

$$f(\vec{q}) = F[\phi(\vec{r})] \times F[L(\vec{r})] = \frac{1}{\Omega_0} F(\vec{q}) \sum_h \sum_k \sum_l \delta(\vec{q} - h\vec{a}^* - k\vec{b}^* - l\vec{c}^*) \quad , \quad (3.6)$$

where Ω_0 is the volume of the unit cell, and $F(\vec{q})$ is the kinematic scattering amplitude of the unit cell. $F(\vec{q})$ is called the structure factor and given by equation (3.4), where the summation is performed over all the atoms in the unit cell. The vectors \vec{a}^* , \vec{b}^* and \vec{c}^* are called reciprocal lattice vectors, and related to the lattice vector \vec{a} , \vec{b} and \vec{c} by

$$\vec{a}^* = \frac{\vec{b} \times \vec{c}}{\vec{a} \cdot (\vec{b} \times \vec{c})}, \quad \vec{b}^* = \frac{\vec{c} \times \vec{a}}{\vec{a} \cdot (\vec{b} \times \vec{c})}, \quad \vec{c}^* = \frac{\vec{a} \times \vec{b}}{\vec{a} \cdot (\vec{b} \times \vec{c})} \quad .$$

The equation (3.6) describes a three-dimensional lattice in the reciprocal space. It can be interpreted in the following way. The diffracted amplitude has a nonzero value only when \vec{q} coincides with one of the vectors

$$\vec{g} = h\vec{a}^* + k\vec{b}^* + l\vec{c}^* \quad . \quad (3.7)$$

This is known as the Laue condition. The three indices h , k and l , when having no common factors larger than 1, are called Miller indices. (hkl) denotes the family of lattice planes perpendicular to \vec{g} , and the space between the planes is equal to $d = 1/|\vec{g}|$. The notation $\{hkl\}$ denotes all planes that are equivalent to (hkl) by the symmetry of the crystal. In addition, $[hkl]$ denotes a direction in the basis of the direct lattice vectors instead of the reciprocal lattice, and $\langle hkl \rangle$ denotes all

directions that are equivalent to $[hkl]$ by symmetry.

Another commonly used interpretation for diffraction from the crystals is Bragg's law. It views the diffracted waves as scattered from different crystallographic planes and construction interference occurs when

$$2d_{hkl} \sin \theta = n\lambda \quad ,$$

where θ is the angle between the incident wave and the family of lattice planes (hkl) and d is the distance between the planes. And the angle, θ , which satisfies this equation is called the Bragg angle. It is easy to show that Bragg's law is equivalent to the Laue condition.

The geometry of the diffraction pattern formation can be expressed by the Ewald sphere construction in reciprocal space as shown in figure 3.1(A). The wave vector \vec{k}_0 of the incident electron beam is drawn from point P to the origin O in the reciprocal space. A sphere of radius k is drawn centered at P. Then for any point Q on the sphere, the reciprocal vector it represents satisfies the relation $\vec{q} = \vec{k} - \vec{k}_0$, where the radial vector from P to Q represents the wave vector \vec{k} of the diffracted beam. The intensity of this diffracted beam is proportional to $|f(\vec{q})|^2$, with $f(\vec{q})$ as scattering amplitude in the reciprocal space at the point Q. This sphere is called Ewald sphere, and it gives both the directions and intensities for all kinematic diffracted beams from a given incident beam.

In the case of diffraction by a single crystal, the scattering amplitude $f(\vec{q})$ is given by equation (3.6) and is nonzero only on the node of the reciprocal lattice. That means, the diffracted beams are only in the directions where the reciprocal lattice points lie on the Ewald sphere. It is easy to show that this is the necessary and sufficient criterion for the Bragg or Laue condition. For high energy electrons, the wavelength is short, e.g., 0.0698 Å in our experiment, and the radius of the Ewald sphere is large ($k = 1/\lambda = 14.33 \text{ \AA}^{-1}$) compared to the distance between the adjacent points of the crystal reciprocal lattice, which is on the order of 0.1 Å⁻¹. As shown in figure 3.1, given the spread out of the scattering amplitude and the Ewald sphere

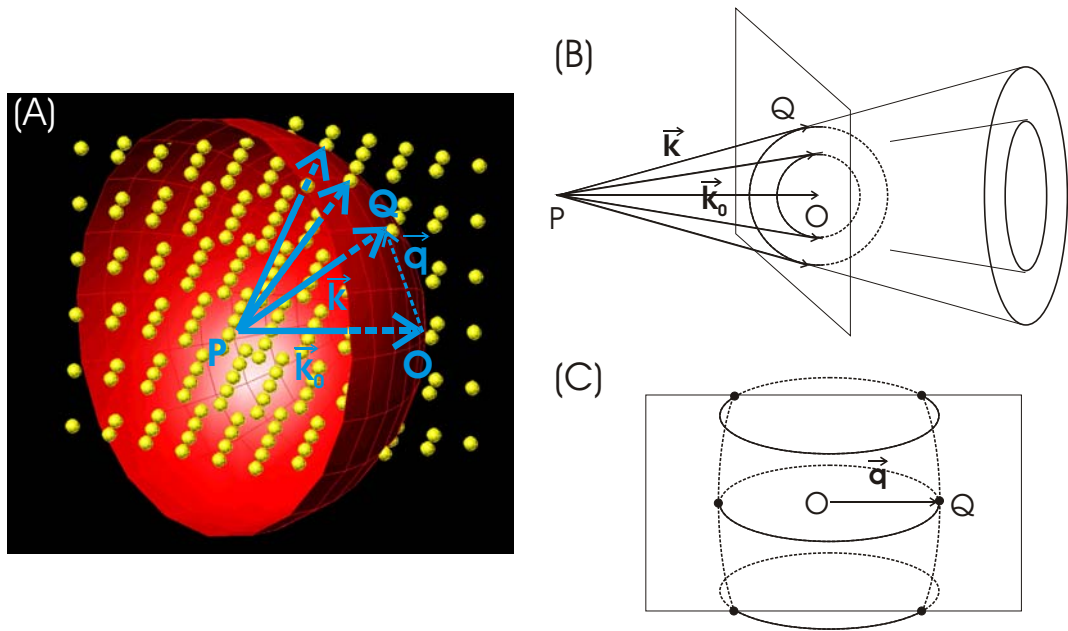


Figure 3.1: Schematic diagrams of the Ewald sphere: (A) for a single crystal in three-dimensional reciprocal space, only half of the Ewald sphere and part of the reciprocal lattice are shown for clarity, also note the reciprocal lattice has intensity modulations as well as systematic absences; (B) for polycrystals; (C) for textured materials.

due to the experimental conditions, a small region around the reciprocal space origin is on the Ewald sphere and represents an almost planar section. The diffraction pattern may thus be recorded on a plane perpendicular to the incident beam and the scatterings which are of interest are predominantly through small angles.

When a diffraction pattern involves multiple electrons, the intensities, not the amplitudes, of individual electron wave function are added. The interactions between different high energy electrons are not coherent [35]. The coherence length of the electron beam is given by the energy and the angular spread [36]. The coherence length of our electrons parallel to the beam direction is given by $l_{\parallel} = 24.5\sqrt{E}/\Delta E = 420$ nm, estimated from the energy spread of $\Delta E = 1$ eV and for the electron energy $E = 30$ keV. The coherence length perpendicular to the beam direction is estimated to be $l_{\perp} = \lambda/\Delta\theta = 1$ nm from the angular spread $\Delta\theta = 7 \times 10^{-3}$ rad. The angular spread also affects the coherence length l_{\parallel} as $l_{\parallel} = \frac{1}{k \sin \theta_i \Delta\theta} = 57$ nm for incidence angle $\theta_i = 1^\circ$, and is the dominant factor.

An ideal polycrystalline material is an assembly of large numbers of randomly oriented crystallites, and is macroscopically isotropic. The effect of randomness is that the reciprocal lattice vectors for a polycrystalline sample lie on a sphere, rather than a set of discrete points for single crystals, as shown in figure 3.1(B). Given by the intersection of these reciprocal spheres with the Ewald sphere, The resulting diffraction pattern is a series of concentric circles around the incident electron direction, which are called Derby-Scherrer rings. Similar to the analysis method introduced previously for gas-phase samples, the radial distribution function for polycrystals can be obtained and gives the distances between the different crystal planes. From these distances, the structure of the crystallites may be derived.

A textured material is a polycrystalline material with intermediate degree of randomness, where the crystallites have some preferential orientation. For example, as often happens in thin films, the crystallites have the same orientation perpendicular to the sample surface, i.e., share a common c -axis. The reciprocal space representation of such a texture consists of a series of rings, and the intersections of the Ewald sphere with the rings form a pattern of spots lying on a series of ellipses (see figure

3.1(C)).

For crystal surfaces and thin films, the lattice is two-dimensional in the surface plane, while the third dimension perpendicular to the surface is very limited. In reciprocal space, the reciprocal lattice is also two-dimensional, as the lattice points elongate in the out-of-plane direction and become lattice rods (figure 3.2). The crystal surfaces are most stable on the dense packed crystal planes (low-indices crystal planes). The surface crystal structure is usually presented following the crystal bulk structure. But the atoms or molecules on surfaces usually reconstruct or relax due to the truncation of the crystal at surfaces and for different adsorbates presented on the surface.

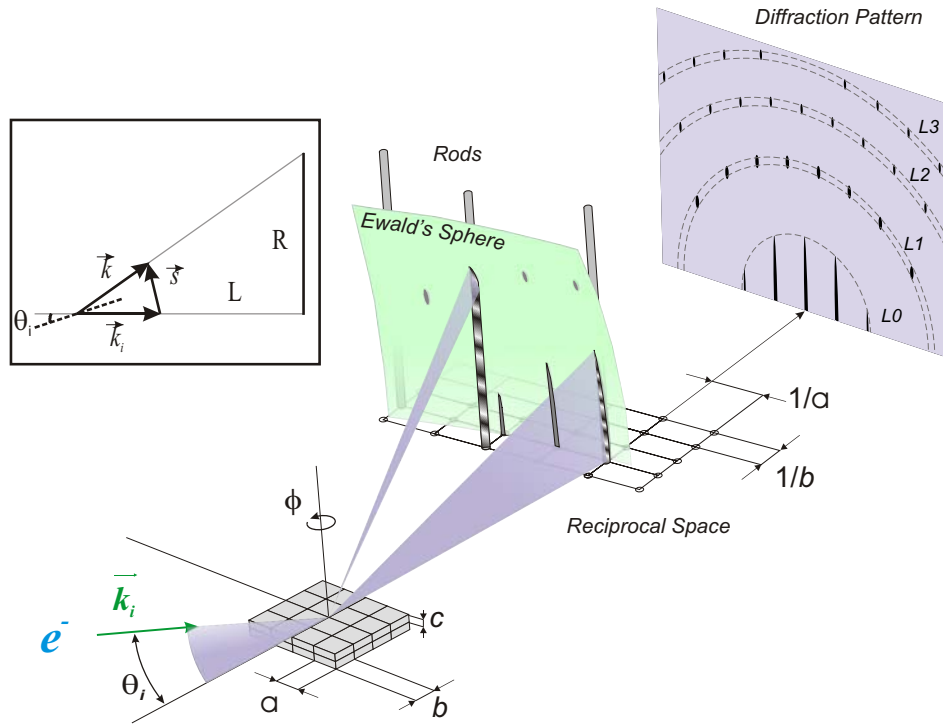


Figure 3.2: Schematic diagram of RHEED experiment, both the Ewald sphere and Laue zones (L_0, L_1, \dots) are displayed [24]. Inset: simplified kinematics of the electron scattering [29].

Because of the large scattering cross section of the electrons, they are ideal for diffraction studies of the surfaces and thin films. When the electron beam incident

at a glazing angle θ_i , which is between the electron beam and the sample surface and usually between 0° and 8° , the electrons penetrate only a few atomic layers into the sample and the diffraction pattern formed by the scattered electrons show the surface structure. This is called reflection high energy electron diffraction (RHEED), a powerful technique to study the surface structures, especially in thin film deposition [37, 38, 36]. With ultrashort time resolution, a whole additional dimension is added for several reasons. First, surface structural changes or restructuring can be probed directly in real time. Second, there is a separation in time scales for motion in the surface layer and perpendicular to it, and initial nonequilibrium (not that of the diffusive regime) structures can be isolated [24]. Third, when the surface is used as a template, substrate-enhanced interferences can be exploited for mapping structural dynamics.

The Ewald sphere construction in RHEED geometry is shown in figure 3.2. The direction of the incident electron beam is defined with respect to a specific crystal orientation (zone axis), where ϕ is the angle between the projection of the electron beam on the sample surface and the zone axis. For a monolayer of atoms in two-dimension, the reciprocal space exhibits “rods” separated by the inverse lattice distances (a and b in figure 3.2). The rods represent the constructive coherent interferences of waves. However, as this monolayer turns into a crystal slab, the rods become modulated, caused by the interlayer spacing (c in figure 3.2). For electrons, Ewalds sphere is large and the diffraction pattern, depending on the incidence angle θ_i , exhibits both the streaks at low scattering angles and Bragg spots at higher angles in Laue zones.

The diffraction intensity can be simulated by using equation (3.5) or (3.6), in which the summations are over the penetrated regions (a few atomic layers) [38, 36]. In practice, a much simplified kinematic scheme of the electron diffraction is often used for crystal surfaces [39], as illustrated in the inset of figure 3.2. The momentum transfer $\vec{s} \equiv \vec{k} - \vec{k}_0$ in reciprocal space satisfies the Laue condition $\vec{s} = h\vec{a}^* + k\vec{b}^* + l\vec{c}^*$, where integers h , k and l are the Miller indices, and \vec{a}^* , \vec{b}^* and \vec{c}^* are reciprocal lattice constants. The value of $s = |\vec{s}|$ is given by $s = 2k \sin(\theta_i)$, and $\tan(2\theta_i) = R/L$, where R is the distance between the diffraction spot and the main beam position on

the screen and L is the distance between the sample and the screen, i.e., the camera length. When the diffracted angle θ_i is very small, which is the case in RHEED, $\sin(\theta_i) \approx \theta_i$ and $\tan(2\theta_i) \approx 2\theta_i$, and the momentum transfer is simply

$$s = k \cdot R/L \quad . \quad (3.8)$$

In RHEED geometry, transmission diffraction through three-dimensional islands or sharp edges is possible [37]. The transmission diffraction patterns are from the bulk reciprocal lattice, have different arrangements of diffracted beams and different behavior as a function of incidence angle comparing to the reflection diffraction. It was observed in our experiments of Langmuir-Blodgett films, as shown in chapter 5.

As a result of the strong interaction between a crystal and high energy electrons, multiple scattering of electrons can not be neglected for the quantitative analysis of the diffraction intensities. The dynamical theory, based on a Bloch-wave solution of the Schrödinger equation for one electron and a crystal potential, has to be utilized, with absorption effects taken into account as the imaginary part of the crystal potential [3, 33, 34, 36].

3.2 Pump-probe experiment

UEC is a pump-probe experiment, as illustrated in figure 3.3. We use a femtosecond laser as pump pulse to initiate the dynamics and to define the zero point in time. The ultrafast electron pulse is used as the probe pulse, which comes in at delay time Δt . Because the interaction of the electrons and sample atoms is very short even on the ultrafast time scale, the diffraction pattern generated by the electron pulse is from the sample atoms at time Δt and represents the dynamical structure at that time. By varying the delay time Δt between the laser pump pulse and the electron probe pulse, a series of the diffraction patterns are recorded. And the analysis of the diffraction patterns map out the structural dynamics as it happens.

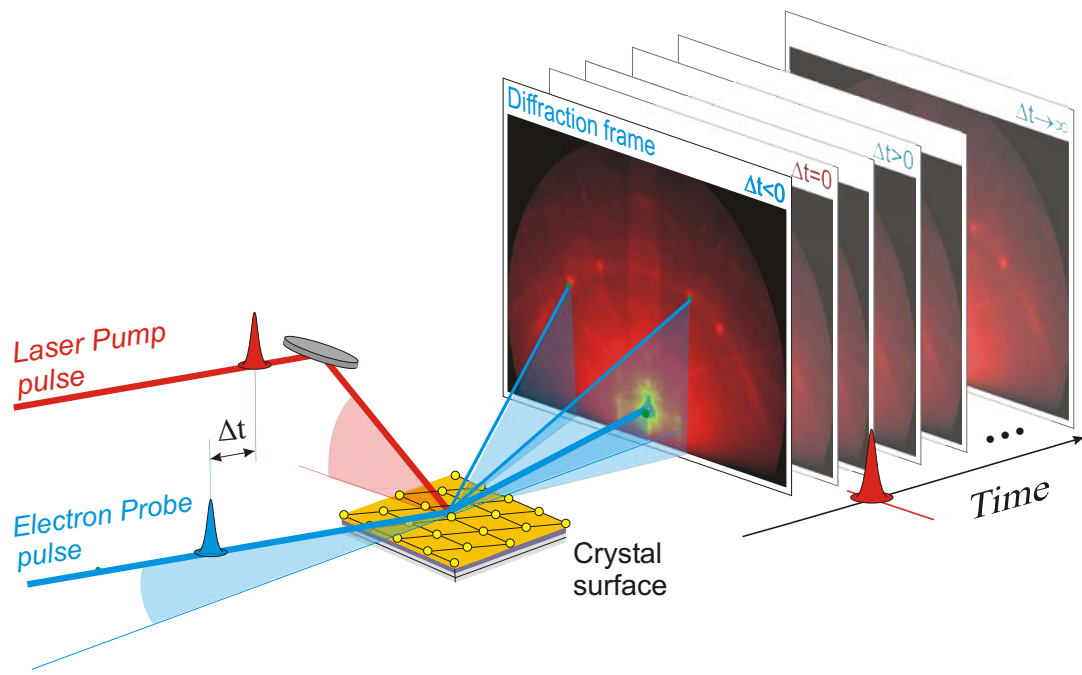


Figure 3.3: Schematic view of the experiment, showing the laser pump and the electron probe pulses, together with typical diffraction frames [25].

3.2.1 Characterization of the electron pulses

The number of electrons in each pulse is linear to the total intensity (I_{et}) of the electron pulse recorded on the CCD camera, $N = I_{et}/I_{es}$, where I_{es} is the intensity produced by a single electron. The intensity I_{es} is a function of the voltage of the image intensifier and is measured as follows. After attenuate the laser (266nm) on photocathode to very low fluence, only a few electrons are generated per pulse and most of them arrive at well separated region on the CCD camera. The intensity of a single electron, I_{es} , is then measured on the screen and statistically satisfies Poisson distribution.

The spatial profile of the electron pulse is measured on the CCD. The electron beam profile on the CCD is Gaussian, and the general diameter (width in one dimension) of the electron beam in UEC experiments is about 500 μm on the CCD.

The temporal width of the electron pulses is characterized in the streaking experiments. Just like in a streak camera, the temporal profile of the electron pulses is transformed into a spatial profile on the CCD, by deflection under a time-varying electrical field, as shown in the inset of figure 3.4. The resulting image forms a “streak” of electron pulses, from which the temporal width is inferred.

In our setup, the time-varying field is provided in the deflection plates (see figure 2.5) through the RC circuit shown in figure 3.4. To get the streaking speed on the order of 1 kV/ns, the resistor R is chosen to be 2 M Ω , and the capacitor $C \simeq 0.01 \mu\text{F}$. The photo-conductive switch is homemade by GaAs semiconductor wafer. When the 800nm laser pulse illuminate the wafer (see the optics layout in figure 2.9), the large electric field breaks the semiconductor and it becomes conducting.

The result of the streaking experiment for our electron gun is shown in figure 3.5. The linear relationship between the electron pulse length and the electron density (see figure 3.5(B)) shows that our electron pulse length is mainly restricted by the space charge effect. This curve only depends on the electron gun configuration, and the fitting line is characteristic of the electron gun. To determine the electron pulse length τ of each experiment, the electron numbers are counted for single pulses. The

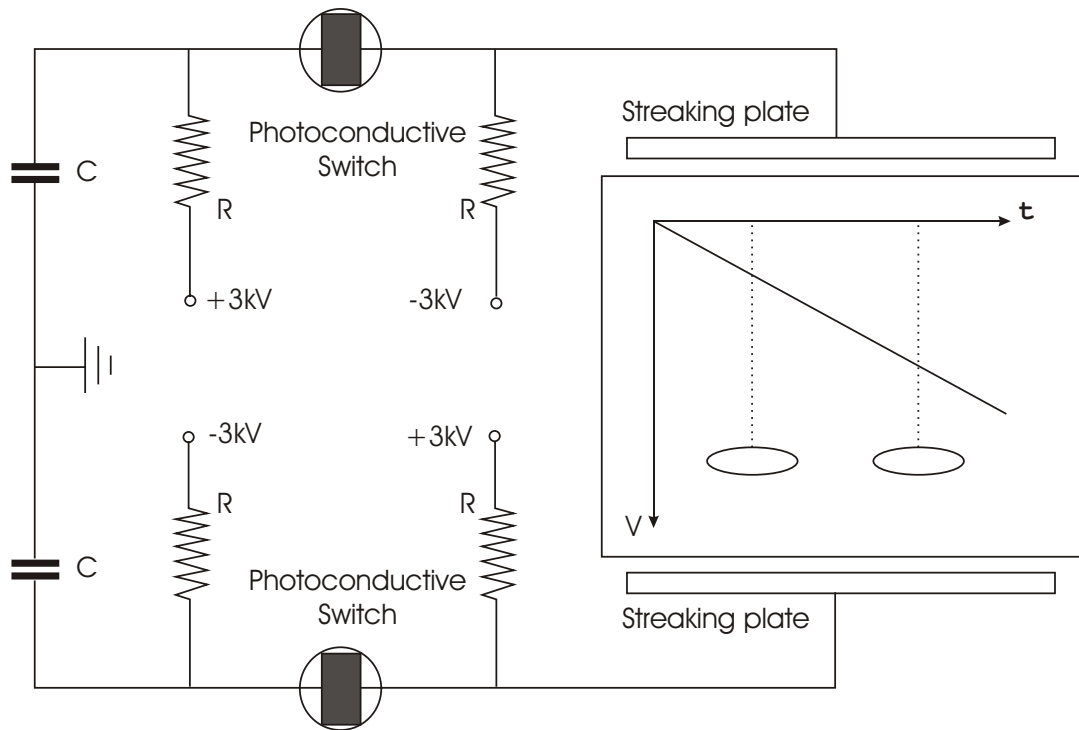


Figure 3.4: The electric diagram for the streaking experiment, the inset inside the streaking plates showing schematic view of streaking.

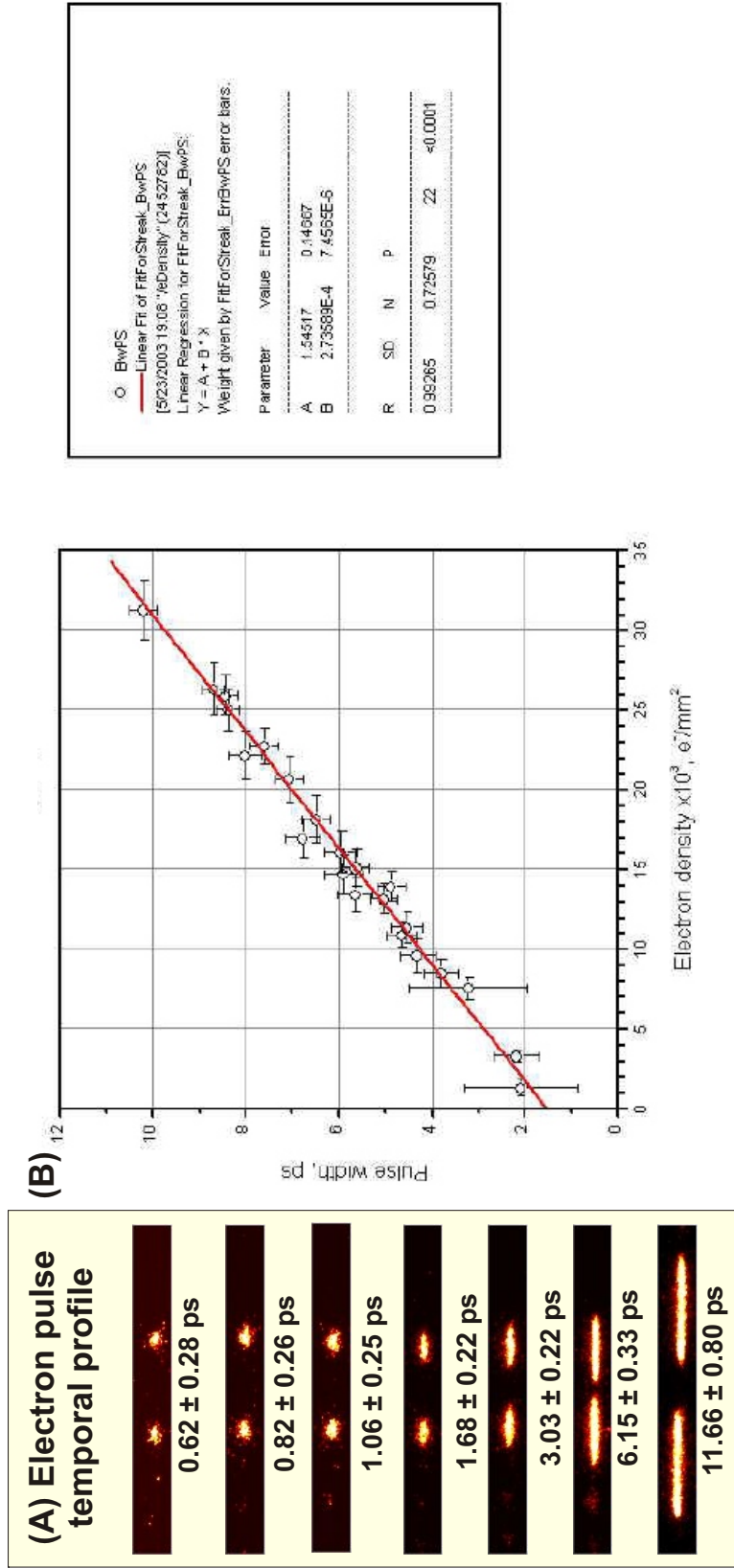


Figure 3.5: Result of the streaking experiment: (A) the streaked electron pulses are displayed for different pulse length [24]; (B) the electron pulse length as a function of the electron density.

electron density per pulse is derived from the electron numbers and the averaged electron spatial area on the CCD. τ is determined by interpolation on the line given by the streaking experiment. On the other hand, in order to get different electron pulse length, the power of the 266nm laser for the electron gun is varied to obtain corresponding electron numbers.

3.2.2 Alignment of the laser and electron beams

Because the electron beam is invisible on the sample, a stainless steel needle and two diode lasers (from Lasermate Group) are used to help to spatially overlap the ultrafast laser beam and the electrons on the sample, as shown in figure 3.6(A). The stainless steel needle is inside the chamber and at the side of the sample holder (see figure 2.4). The needle tip defines a point in space where the two diode lasers shooting from two different directions, the ultrafast laser beam and the electrons are brought on respectively.

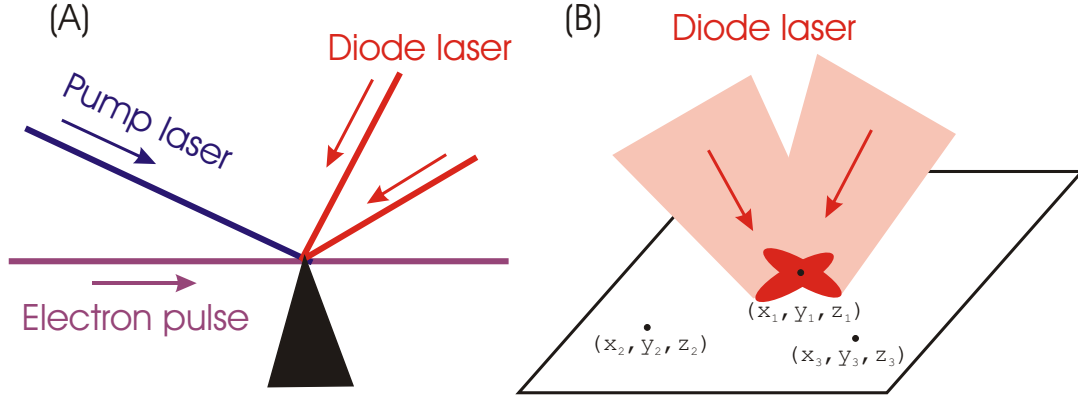


Figure 3.6: Schematic diagram of the alignment: (A) the overlap of the electron beam, the fs laser beam and two diode laser beams on the tip of the needle; (B) three-point alignment of the two diode laser to determine the sample surface plane.

After all four beams overlap on the needle tip, the sample is moved in position. The diode laser beams shoot on the sample and leave two prints (figure 3.6(B)), which are monitored through a viewport by a color CCD camera (JAI high resolution CCD camera with 75 mm focusing lens from Edmund Optics, Inc., Barrington, NJ) outside

the chamber. The sample has five degrees of freedom. They are three in translation, x , y and z ; out of plane rotation θ and in plane rotation ϕ . With fixed θ angle, the sample surface is a fixed plane in space. At the fixed position x and z , varying y can bring the two diode laser beams to overlap on the sample. This position on the sample surface is the same position where the needle tip was, and where the electron beam and the excitation fs laser beam overlap in space. This position is now defined by the coordinate (x_1, y_1, z_1) . Move the sample to another position with different x and z , and by changing y again bring the two diode laser beams overlap on the sample surface. This determines the second point (x_2, y_2, z_2) . Following the same procedure, a third point can also be determined at (x_3, y_3, z_3) . These three points thus define the sample surface plane at angle θ .

Using the same method, a plane at a different θ angle can also be found. The crossing line of these two planes is the axis around which θ is rotated. Thus we find the relationship between the goniometer motion system and the overlap of the electron beam and the excitation fs laser beam in space. At any point on the sample surface when the sample is at any given θ , we can calculate the coordinate which is required for the x , y , z motion to bring it to the overlap with the electron beam and the laser beam. We call this the three-point alignment.

In practice, we do the alignment at three different angles to check the relative accuracy of the determination. When doing experiments, after finding dynamics, we can move y a little bit to optimize for the overlap by optimizing the change of diffraction patterns.

3.2.3 Measuring the laser fluence on the sample

In order to determine the excitation laser fluence at the sample position, the laser power and the area of the laser illumination on the sample are measured individually.

Without the sample, the excitation laser power is measured right before entering the vacuum chamber (I_{total}) and right after shooting out from the other side (I_{out}) to determine the absorption I_a of the vacuum chamber windows $I_a = (I_{total} - I_{out})/2$. With the sample, the laser power I_{total} and I_{out} (after reflection) are measured again.

And the excitation laser power absorbed by the sample surface is given by $I = I_{total} - I_{out} - I_a$.

To measure the area of the laser illumination on the plane of the sample surface, the needle used for alignment is utilized. As shown in figure 3.7, assuming a round beam cross section with the radius r being the full width at half maximum (FWHM) of the Gaussian profile, the laser footprint on the xz plane (sample surface) is an ellipse with area

$$A = (\pi r^2) / \sin \theta \quad ,$$

where θ is the angle between the laser beam and the xz plane. The needle is in the xy plane as shown in figure 2.4. By moving the needle in x direction, with enough height in y direction, the laser beam is blocked by the needle, starting from position x_1 and ending at x_2 . It is calculated that the relationship between the measured length $l_x = x_2 - x_1$ and r is

$$2r = l_x \sin \Phi \quad , \quad (3.9)$$

where Φ is the azimuthal angle in the xz plane (see figure 3.7). The calculation is not straightforward although the result is simple. The needle measures the projection of the laser on the xy plane, which is an ellipse with angles θ' and Φ' where $\sin \theta' = \cos \theta \sin \Phi$ and $\sin \theta = \cos \theta' \sin \Phi'$. The equation of the ellipse in the xy plane is $(x \cos \Phi' + y \sin \Phi')^2 \sin^2 \theta' + (y \cos \Phi' - x \sin \Phi')^2 = r^2$. And the point of x_1 and x_2 satisfy the equation $(x \cos \Phi' + y \sin \Phi') \sin^2 \theta' \sin \Phi' + (y \cos \Phi' - x \sin \Phi') \cos \Phi' = 0$. The result (3.9) is obtained by solving the above equations.

3.2.4 Determining time resolution and time zero

The time resolution of UEC is determined by the laser pulse duration, electron pulse duration and the geometrical effect. Because of the group velocity dispersion, after traveling through the beam path (figure 2.9), the 120 fs laser ($\lambda = 800$ nm) pulse broaden to approximately 200–300 fs. Since the electron pulse is generated by the fs laser pulse, its pulse length is equal to or larger than the fs laser pulse length. But our electron pulse length is limited by the space charge effect, as shown by our streaking

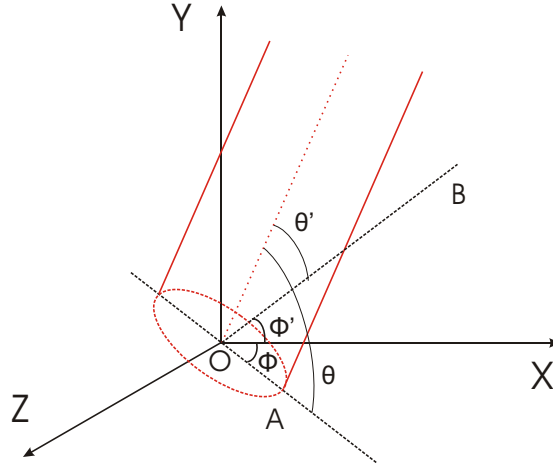


Figure 3.7: Schematic diagram of the measurement of excitation laser beam spatial profile.

experiment (see 3.2.1). In typical UEC experiments, electron pulses of 4–5 ps are used with ~ 3000 electrons per pulse. So the electron pulse width and the geometrical effect are determining factors.

In the case of transmission, the sample is very thin (~ 100 nm). The time it takes for the electrons to travel through the sample is 1 fs for the $1/3$ speed of light, which is the speed for our 30 keV electrons. So the time resolution is determined by the electron pulse duration. In this case, because of the high density of the atoms, fewer electrons can be used to get relatively good diffraction patterns. That brings shorter pulses and so better time resolution.

In the case of reflection, however, the geometrical effect is more important. The beam profile at the sample is about $250 \mu\text{m}$. At the incidence angle of 1° , the electron beam on the sample is 14 mm long. The laser beam profile on the sample, i.e., the excited area, is about 1 mm, which yields a group velocity dispersion (GVD) of 10 ps. To increase the time resolution, one way is to reduce the GVD by reducing the spatial extent of the sample by masking techniques [25]. With convolution and the strong level of signal from crystal surfaces, we readily obtained a 1-2 ps response. Another

way is to match the group velocity of the excitation laser pulse with the GVD of the electron pulse [32].

The time zero is determined *in situ*. However, it obscures any delay that may exist between the fs laser excitation and the start of the structural changes, as for example observed in InSb [40, 41]. Another method to determine time zero is to use the plasma lensing effect from the stainless steel needle [42, 43, 32]. It is shown that after the fs laser shoot on the needle, there is a charging effect which shifts the electron beam. It can determine the time zero to within 1 ps, but needs a lot of laser power and can destroy the needle tip.

3.3 Analysis of the diffraction patterns

The diffraction pattern recorded on the CCD represents an almost planar section in the reciprocal space. The corresponding reciprocal space distance to the distance on the screen is given by equation (3.8). The camera distance L , is the distance between the footprint of the incidence electron beam on the sample and the phosphor screen. It is determined *in situ*, by the crystal substrate diffraction patterns at varied incidence angles, with known lattice constants for the substrate (in our cases silicon). The direct beam position, i.e., the incidence beam on screen corresponding to $s = 0$ (origin) in reciprocal space, is also determined *in situ* from the substrate diffraction patterns.

Depending on the sample surface crystallinity, the diffraction patterns are very different. The single-crystal or textured surface give diffraction spots or lines, whereas the polycrystal or amorphous surface give Debye-Scherrer diffraction rings. The analysis is different in the two cases.

When the sample surface is single-crystal or textured, the diffraction patterns contain diffraction spots or lines. The positions of the spots are determined by the crystal structure and the sizes (or the widths) show the states of defects in the crystal. The structural dynamics can be revealed by following the change in the positions and the sizes of the spots. To determine the position and the width accurately, especially

in the case when the change is very small, the spot or the line is fitted by a Voigt peak function in the direction of interest. Voigt function is the convolution of a Lorentz function and a Gaussian function. It is the best fit of our diffraction peak in general, though with different coefficient, sometimes the peak is more Lorentzian or Gaussian. The full width at half maximum (FWHM) of a Voigt function is given approximately as

$$(2\omega)^2 \simeq \frac{(2\omega_G)^2}{\ln 2} + (2\omega_L)^2 \quad ,$$

where 2ω , $2\omega_G$ and $2\omega_L$ are the FWHM of the Voigt function, the Gaussian and the Lorentz function [44, 45].

When the sample surface is polycrystal or amorphous, the diffraction patterns contain diffused diffraction rings (half ring or curves on the ring above the shadow edge) with the same center, which is the direct beam position. Similar to the analysis of gas-phase material, the intensity is averaged on the curve (angularly) to get the diffraction intensity as a function of reciprocal space distance $I(s)$.

The intensity of the diffraction spots or rings are usually the first sign of structural change. In thermal equilibrium states, the intensity change with temperature is explained by Debye-Waller effect [34]. In reciprocal space, the effect of thermal vibration on the average potential can be described by

$$F_s = \sum_j f_j^{(e)} T_j \exp(i\vec{s} \cdot \vec{r}_j) \quad .$$

The temperature factor T_j is given by $T_j = \exp(-\frac{1}{2} \langle (\vec{s} \cdot \vec{u}_j)^2 \rangle)$, where \vec{u}_j denotes the instantaneous displacement of the j-th atom from its equilibrium position, and $\langle \dots \rangle$ is averaging over thermal equilibrium. For isotropic thermal vibrations, $\langle (\vec{s} \cdot \vec{u}_j)^2 \rangle = \frac{1}{3} s^2 \langle \vec{u}_j^2 \rangle$ and

$$T_j = \exp[-B_j s^2 / (16\pi^2)] \quad ,$$

where $B_j = \frac{8}{3} \pi^2 \langle \vec{u}_j^2 \rangle$ is the Debye-Waller factor and B of many materials have been determined by theories and experiments. For a lot of simple crystals,

$B(T) \simeq a_0 + a_1T$. The total integrated intensity of a diffraction spot then satisfy the relationship

$$\ln\left(\frac{I(T)}{I(T_0)}\right) = -2[B(T) - B(T_0)]s^2 \quad .$$

However, since UEC is used to study the structural dynamics, the diffraction patterns are of samples in highly nonequilibrium state. So it could be questionable using the Debye-Waller coefficients, which are determined in the static temperature dependence experiments, to relate the intensity change with the thermal temperature change. Nevertheless, the intensity change gave insights on the orderness of the crystal structure, especially when combined with the widths change of the diffraction spots or rings.

The change with time is fitted with multiple exponential functions [46]. While the state of different structures are straightforward, it is assumed that the change is homogeneous in the probing area. The assumption is valid in the case when the probing area is much smaller than the excited area. In principal, a better theoretical analysis would be simulations using molecular dynamics to determine the atomic structure, and fit the whole diffraction pattern intensity using dynamical theory.